Convection under internal waves in a mountain lake

by Hans van Haren[*1], Henk A. Dijkstra[2]

[1]Royal Netherlands Institute for Sea Research (NIOZ) and Utrecht University, P.O. Box 59, 1790 AB Den Burg, the Netherlands.
*e-mail: hans.van.haren@nioz.nl

[2]Institute for Marine and Atmospheric research Utrecht, Department of Physics, Utrecht University, Utrecht, the Netherlands.

ABSTRACT

Turbulent mixing processes in deep alpine Lake Garda (I) have not extensively been observed. Knowledge about drivers of turbulent fluxes are important for insights in the transport of matter, nutrients and pollutants, in the lake and in natural water bodies in general. In this paper, the occurrence of internal wave induced turbulent convection is addressed as opposed to the more common shear-induced turbulence in a density stratified environment. Observations are analyzed from a dedicated yearlong mooring holding 100 high-resolution temperature sensors at 1.5 m intervals under a single current meter in the deeper half of the 344 m deep lake-center. Episodically, the weakly density stratified waters in the lower 50 m above the lake floor show spectral slope and coherence evidence of short-term (15 to 30 minutes) convective motions under internal waves that are supported by the stronger stratified waters above. The near-homogeneous conditions are not attributable to frictional Ekman dynamics, but to large-scale internal wave crests.

I. INTRODUCTION

'Natural (free)' turbulent convection is generally considered to occur during a period of gravitational instability when denser (relatively cool) fluid is over less dense (warmer) fluid [Sharp (1984), Kull (1991), and Dalziel (1993)]. It is a very efficient mixing process (Dalziel *et al*., 2008) and therefore important for fluxes of nutrients and suspended particles in geophysical environments like the atmosphere and ocean. Natural convection commonly occurs in the atmosphere during daytime heating due to solar radiation reflecting from the Earth surface below. This turbulence process is classically studied in a laboratory oil-filled pan over a heat source as Rayleigh-Bénard convection (e.g., Getling, 1998). The convection is characterized by up- and down-ward cells of motion that have an aspect ratio (of vertical over horizontal dimensions) of approximately unity (Christensen and Yuen, 1988). Commonly, ocean turbulence has more than one (overturning-)cell-size, in fact many from the large (>100 m) energy containing scales to the 0.001 m dissipation scales. The spatial pattern of such convection is up- and down-ward motions of less dense and denser fluids at the largest scale again with an aspect ratio close to unity. The large-scale motions are irregular along the edges due to secondary and smaller-scale motions.

While natural convection drives the atmospheric boundary layer turbulence, mainly during daytime, and is well-established in driving the nighttime (cooling) near-surface ocean turbulence (e.g. Brainerd and Gregg, 1993), it has not often been observed in the deep ocean. This is because of the dominant vertical density stratification in the deep ocean due to the large daytime solar heating from above, in spite of geothermal heating from below (e.g, Wunsch, 2015). Apparently for geothermal heating (less than 1% of solar heating, Mullarney *et al*., 2006) to be observed directly, one requires homogeneous waters near the ocean-floor and weak horizontal density gradients and horizontal currents. Near-homogeneity is a rare phenomenon in the ocean, and which requires high-resolution observations to be able to record, e.g., temperature differences of less than 0.1 mK.

Natural convection is known to only occur when gravity is overcome, either by an unstable set-up as in Rayleigh-Bénard convection, or, in a laboratory, by applying bulk

forcing acceleration of an entire container with a stably stratified fluid exceeding 1g (e.g., Olson and Jacobs, 2009), g denoting the acceleration of gravity. Internal waves usually do not accelerate over 1g, but they may overcome 1g', for reduced gravity $g' = g\Delta\rho/\rho$. The rationale would be an internal forcing generation, not a bulk forcing, of natural convection in a stably stratified fluid, as suggested for a similar observation under ocean internal waves (van Haren, 2015). One could term this 'internally forced convection'.

In this paper, the phenomenon of internally forced convection in Lake Garda (I) is evidenced in substantial observational detail by contrasting it with a shear-dominated case one day later in the records of moored temperature sensors.

II. SITE AND DATA

Lake Garda is an approximately 40 km long and 5 km wide lake roughly directed north-south, with depths up to 346 m. For one year a taut-wire sub-surface mooring was installed near its deepest point, at latitude 45° 42.947′N ($f = 1.04\times10^{-4}$ s^{-1}, providing $T_f = 16.7$ h), longitude 10° 44.567′E, between 10 UTC on 24/05/17 (yearday 144.42) and 09 UTC on 31/05/18 (yearday 516.37; days in 2018 are +365). The local water depth H = 344 m with a relatively weak bottom slope (100 m scale) of about $\beta = 3°$. At a distance of 300 m to the East and 1.3 km to the West, the lake floor shallows with slopes varying between 10° and 20°.

The mooring consisted of floatation near its top providing 1100 N net buoyancy. Below the floatation, a single point Nortek AquaDopp current meter was at z = -187 m, sampling current components [u v w] and storing ensemble data every 300 s. The current meters' tilt and pressure sensors demonstrated that the mooring-top did not move more than 0.05 m vertically and not more than 5 m horizontally, under maximum current speeds of 0.17 m s^{-1}. Typical current speeds vary between 0.01 and 0.05 m s^{-1}.

In the vertical range $-338 < z < -189.5$ m, 100 'NIOZ4' self-contained high-resolution temperature T-sensors were located at 1.5 m vertical intervals, sampling at a rate of once per 2 s. NIOZ4-sensors have a precision of better than 0.5 mK after drift correction, a noise level

of less than 0.1 mK and a resolution of less than 0.01 mK (van Haren, 2018). The T-sensors are synchronized via induction every 4 hours and a vertical profile of 148.5 m is measured in less than 0.02 s.

Drift of nominally 1 mK/mo for aged sensors is corrected by fitting typically 4 day mean temperature profiles to a smooth statically stable multiple order polynomial profile. The mean profile is tuned with local shipborne Conductivity, Temperature Depth (CTD-)profile data obtained roughly once every 6 weeks by the Environmental Protection Agency of the Veneto Region within 1 km from the mooring site. Up to day 350, 7 sensors showed various electronic (noise, calibration) problems and are not further considered. The measured temperatures are transferred to Conservative Temperature Θ to correct for pressure-compressibility (IOC *et al.*, 2010). As the observations were made in a freshwater lake with minimum temperatures of about 8 °C (>4 °C of maximum density), the temperature-density relationship is always tight. Salinity contributes at best a factor of 30 less than temperature to density variations, as has been verified with the CTD-data. Further details on the site and mooring details, together with an overview of the entire observational period can be found in van Haren *et al*. (2019; submitted).

III. OBSERVATIONS

Up- and downward motions with aspect ratio of about 1 and irregular along the edges, are observed under small-scale internal waves in mountain Lake Garda (Fig. 1). However, the image is upside-down with respect to one of natural convection, as the instabilities are slightly larger at the warmer, stable side. In this large magnification of Eulerian high-resolution temperature observations it is seen, with the aid of transferring the horizontal time-axis into a spatial axis using the mean mid-depth current speed, that the approximately 15 minute scale motions are roughly 20 m large. All characteristics point at convective, not shear-induced turbulent overturning. However, the convection occurs in a larger-scale stable stratification under internal wave action. It is noted that the present freshwater Lake Garda temperature

data in Fig. 1 are undisputed tracers for density variations, unlike observations from the ocean where salinity also may contribute to density variations.

A. Contrasting examples of shear and convective turbulence under internal waves

Energy and coherence spectra are used to qualitatively support the analysis on the two specific turbulence processes of convective and shear-induced overturning. The results are presented for 1.5 days occurring in mid-November about one day after the onset of a relatively strong northerly wind (blowing to the south). Such northerly wind events occur episodically roughly every 10 days and exert a rapid several tens of meters deep depression of the stratification (van Haren *et al*., 2019). Upon the relaxation of such a depression, a train of high-frequency internal waves occurred over a weakly stratified layer lasting two inertial (16.7 h) periods, each inertial period demonstrating distinctly different turbulence in the lower layer of dominant shear-induced overturning (Fig. 2) and convective overturning (Fig. 3). Fig. 1 is a magnification of the inertial period of Fig. 3.

A.1. Correspondence between the two inertial periods

Both inertial periods have in common that the larger stratification (Fig. 2a, 3a) in the upper 45 m layer of the sampled range is reflected in larger temperature variance compared to that of the lower near-bottom layer (Fig. 2d, 3d). In the second half of each image (Fig. 2a, 3a), both inertial periods demonstrate a weakly (minimum) stratified layer with mean $N = 2f$ that lasts about half an inertial period and which extends about 40 to 50 m above the lake floor, while varying over shorter timescales. The average Ozmidov scale of largest overturn in a stratified environment is smaller for the upper layer than for the lower layer, being smaller than and larger than the 1.5 m separation distance between the T-sensors, respectively. Both inertial periods show a gradual decrease in coherence for frequencies $\sigma > N$ at all depths (Fig. 2e, 3e). Both inertial periods also show less coherence in the well-stratified upper layer compared to the weakly stratified lower layer, not only at the smallest 1.5 m scale displayed in Fig. 2e, 3e, but also at larger scales, for all $\sigma > N$. Details however, vary between the two

inertial periods that are attributable to different predominant turbulence processes in the lower layer.

A.2. Differences between the two inertial periods

The inertial period in Fig. 2 shows less hair-like variations in temperature (stratification) in the lower layer up to 50 m above the lake floor (Fig. 2a,b), up to one order of magnitude less variance (Fig. 2d), and less coherence (Fig. 2e), compared with the inertial period of Fig. 3. In the upper layer in more stratified waters of Fig. 2, the temperature variance shows a broad peak around the first inertial higher harmonic 2f. This peak is absent in Fig. 3d. If associated with near-inertial waves, as a first harmonic, they may be associated with near-inertial shear. Such a shear is the dominant shear in stratified seas because of the short vertical length scales of near-inertial waves (e.g., LeBlond and Mysak, 1978). This potential of near-inertial shear may explain the near-lake floor spectrum being close to the $\sigma^{-5/3}$-scaling of inertial subrange turbulence of a passive scalar in Fig. 2d [(Tennekes and Lumley (1972), and Warhaft (2000)], throughout the range $\sigma > N_{max}$, the local maximum small-(1.5 m) scale buoyancy frequency.

The inertial period in Fig. 3, with overall mean turbulence level of about twice that of Fig. 2 (van Haren *et al*., 2019), is characterized by a growing of the weakly turbulent layer near the lake floor with apparent convection type up- and down-ward turbulence motions of which the scales have an aspect ratio of about 1 (cf. Fig. 1). The 20-m, 100 cycles per day (cpd) scale motions are indeed found significantly coherent at the 1.5 m T-sensor separation (Fig. 3e). However, much higher frequency motions are still found coherent (at the 1.5 m scale), down to about 2000 cpd. The corresponding temperature variance spectrum, which is much more energetic over a broad range $\sigma > 2f$ than in Fig. 2, does not follow the $\sigma^{-5/3}$ scaling law of shear-induced turbulence (Fig. 3d). For $\sigma < 1000$ cpd the spectral slope (on the log-log plot) is less steep than -5/3, while for $\sigma > 1000$ cpd it is steeper than -5/3. The different spectral slopes in Fig. 2d and Fig. 3d distinguish convection from shear dominance in turbulent overturning (Cimatoribus and van Haren, 2015). These deviations from the inertial subrange $\sigma^{-5/3}$ scaling point at convective turbulent overturning of an active scalar. The

portion $\sigma > N$ of the upper layer (high variance, stronger stratified environment) spectrum is closer to the $\sigma^{-5/3}$ scaling of a passive scalar.

IV. SUGGESTIONS FOR INTERNAL WAVE CONVECTION GENERATION

It remains to be discussed why internally forced convection is mainly observed in the lower 50 m above the lake floor when high-frequency internal wave activity is rather intense in Figs 1,3. The weakly stratified layer near the lake floor cannot be generated by <0.1 m s^{-1} frictional flows, which would yield a near-homogeneous layer of only a few meters thick (Ekman, 1905). Several possibilities exist for internal waves to generate the weakly stratified conditions and convective turbulence over vertical ranges of several tens of meters above the lake floor, as sketched in Fig. 4.

One suggestion is that propagating high-frequency internal waves strain the stratification, which results in alternate phases with larger than average stratified waters in a thin layer close to the lake floor following downward motions with less than average stratification following upward motions (Fig. 4a). The latter may serve as a preconditioning of sufficiently weakly stratified waters in which convection can penetrate during the downward phase. The solid boundary of the lake floor acts as a one-sided restricting limit for the straining of isopycnals.

An alternative suggestion is inspired by Thorpe (1994, 2010) who proposed internal wave breaking patches with convective overturning in obliquely propagating internal waves in the ocean interior (Fig. 4b). In a similar fashion, nearby sloping topography as in the lake's sidewalls may favour strongly non-linear internal wave propagation and associated patches of, possibly intensified, convective turbulence.

Such convective instabilities under obliquely propagating (non)linear internal waves may interact with rotational physics processes. For example, McEwan (1973) suggested 'inertial' gyroscopic wave breaking providing columnar vortices and, possibly, yielding slanted convection [Straneo *et al*., (2002), and Sheremet (2004)]. The convection will be, for pure homogeneous water, in the direction of the Earth rotational vector. At mid-latitudes, this will appear as weakly stratified water ($N = f, 2f, 4f$, depending on the prevailing stability

mechanism, van Haren (2008)). In the present observations, N = 2f dominates in the weakly stratified layer near the lake floor.

V. GENERAL DISCUSSION

The observations on convective mixing under internal waves in the deeper weakly stratified part of Lake Garda demonstrate the richness of turbulence generation phenomena in geophysical environments. It is noted that in these observations temperature is a unique tracer for density variations and that geothermal heating from below is not relevant. Several hypotheses about generating convection in a weakly stratified environment were postulated.

It seems that the accelerations of the observed convective turbulence, in combination with the internal wave vertical motion variations, can overcome reduced gravity to sufficiently penetrate the stable weakly stratified layer below. Reduced gravity $g' = g\Delta\rho/\rho \approx 2gA$ is the natural driving force for internal waves in stable-stratified fluids. The Atwood number $A = \Delta\rho/\Sigma\rho$ denotes the ratio of the density (ρ) difference across an interface and the sum of the different densities in both layers above and below the interface (Dalziel, 1993). In Lake Garda $A \approx -10^{-7}$, roughly calculated following the observations in Figs 1,3 after conversion of temperature into density variations, and it is proposed that g' should replace g in considering accelerations to overcome stable stratification (van Haren, 2015). As the present wave-induced penetration has vertical motion variations of $\Delta w \approx 0.01$ m s^{-1}, the condition for the magnitude of its accelerations is $|\Delta w/\Delta t| = a_w > g'$, which is satisfied when $\Delta t < 3000$ s. This time-variation limit is close to the observed minimum buoyancy period in Figs 1,3, or the largest turbulence timescale of the entrainment overturns observed. The correspondence with the minimum buoyancy frequency is similar to ocean observations (van Haren, 2015), in which values were an order of magnitude different from the ones presented here.

The overcoming of reduced gravity in internally forced convection by internal waves as opposed to gravity in bulk forcing of an entire water basin is rationalized in analogy of parcel displacement leading to the buoyancy frequency definition (Groen, 1948). After all, in a

stably stratified environment the vertical displacement of a parcel of density ρ yields a restoring force g' that sets high-frequency internal waves into motion at N.

The internally forced convection of a stratified fluid has a peculiar characteristic in that when it is forced at $a_w > g'$, it will reinforce itself by its secondary shear-induced mixing that entrains heavier fluid in a downward going column that is less dense than the environment. This reduces the density difference between column and environment, until the difference disappears at the deepest point of the column. This process is at odds with natural convection, which requires continuous (bulk) forcing by gravity as a downward going denser column will entrain less dense fluid from its statically unstable environment, thereby counteracting the convective motion. Semantically, internally forced convection is more natural.

The two inertial periods demonstrating different dominating turbulence are observed in sequential order following a sudden wind-event disturbance. The first day after the initiating strong depression of isotherms, intense high-frequency internal occur under which a dominance of large-scale convection is observed. An inertial period later, these high-frequency internal waves are considerably reduced except for the first inertial higher harmonic and shear-induced overturning dominates. Further laboratory and numerical modelling is required to test the above suggestions and which may best explain the presented observations of internally forced convection in weakly stratified waters under internal waves of different frequency. One could create two different excitations of a stratified rotating fluid bounded by weaker stratification below, one exciting near-buoyancy frequency waves, the other near-inertial waves. Or, a large depression is excited and the development is studied in a stratified rotating fluid, in which then also the removal of high-frequency waves may be studied at the expense of near-inertial waves.

ACKNOWLEDGMENTS

We highly appreciate the assistance of the Nautical Rescue Team 'Vigili del Fuoco-Trento', S. Piccolroaz and M. van Haren around the deployment and recovery of the mooring. We thank M. Laan for all his temperature sensor efforts. This project was funded by the Faculty of Science of Utrecht University through a grant to HD and was supported by the National Marine Facilities (NIOZ).

REFERENCES

Brainerd, K. E. and Gregg, M. C., "Diurnal restratification and turbulence in the oceanic surface mixed layer: 1. Observations," J. Geophys. Res. **98**, 22,645-22,656 (1993).

Christensen, U., and Yuen, D., "On the aspect ratio of Rayleigh-Benard convection cells," Geophys. Res. Lett. **15**, 597-600 (1988).

Cimatoribus, A. A., and van Haren, H., "Temperature statistics above a deep-ocean sloping boundary," J. Fluid Mech. **775**, 415-435 (2015).

Dalziel, S. B., "Rayleigh-Taylor instability: experiments with image analysis," Dyn. Atmos. Oc. **20**, 127-153 (1993).

Dalziel, S. B., Patterson, M. D., Caulfield, C. P., and Coomaraswamy, I. A., "Mixing efficiency in high-aspect-ratio Rayleigh–Taylor experiments," Phys. Fluids **20**, 065106 (2008).

Ekman, V. W., "On the influence of the Earth's rotation on ocean-currents," Ark. Math. Astron. Fys. **2(11)**, 1-52 (1905).

Getling, A. V., *Rayleigh-Bénard Convection: Structures and Dynamics* (World Scientific, 1998) p. 256.

Groen, P., "Contribution to the theory of internal waves," K.N.M.I. Med. Verh. **B11**, 1-23 (1948).

IOC, SCOR, and IAPSO, *The international thermodynamic equation of seawater – 2010: Calculation and use of thermodynamic properties* (Intergovernmental Oceanographic Commission, Manuals and Guides No. 56, UNESCO, 2010), p. 196.

Kull, H. J., "Theory of the Rayleigh-Taylor instability," Phys. Rep. **206**, 197-325 (1991).

LeBlond, P., and Mysak, L. A., *Waves in the Ocean* (Elsevier, 1978), p. 602.

Olson, D. H. and Jacobs, J. W., "Experimental study of Rayleigh-Taylor instability with a complex initial perturbation," Phys. Fluids **21**, 034103 (2009).

Mullarney, J. C, Griffiths, R. W., and Hughes, G. O., "The effects of geothermal heating on the ocean overturning circulation," Geophys. Res. Lett. **33**, L02607, doi:10.1029/2005GL024956 (2006).

Sharp, D. H., "An overview of Rayleigh–Taylor instability," Phys. D **12**, 3-18 (1984).

Sheremet, V. A., "Laboratory experiments with tilted convective plumes on a centrifuge: A finite angle between the buoyancy force and the axis of rotation," J. Fluid Mech. **506**, 217-244 (2004).

Straneo, F., Kawase, M., and Riser, S. C., "Idealized models of slantwise convection in a baroclinic flow," J. Phys. Oceanogr. **32**, 558-572 (2002).

Tennekes, H., and Lumley, J. L., *A first course in Turbulence* (MIT Press, 1972), p. 300.

Thorpe, S. A., "Statically unstable layers produced by overturning internal gravity waves," J. Fluid Mech. **260**, 333-550 (1994).

Thorpe, S. A., "Breaking internal waves and turbulent dissipation," J. Mar. Res. **68**, 851-880 (2010).

van Haren, H., "Abrupt transitions between gyroscopic and internal gravity waves: the mid-latitude case," J. Fluid Mech. **598**, 67-80 (2008).

van Haren, H., "Instability observations associated with wave breaking in the stable-stratified deep-ocean," Phys. D **292-293**, 62-69 (2015).

van Haren, H., "Philosophy and application of high-resolution temperature sensors for stratified waters," Sensors **18**, 3184, doi:10.3390/s18103184 (2018).

van Haren, H., Piccolroaz, S., Amadori, M., Toffolon, M., and Dijkstra, H. A., "Moored observations of turbulent mixing events in Lake Garda (I)," Limnol. Oceanogr., subm. (2019).

Warhaft, Z., "Passive scalars in turbulent flows," Ann. Rev. Fluid Mech. **32**, 203-240 (2000).

Wunsch C., *Modern Observational Physical Oceanography: Understanding the Global Ocean* (Princeton University Press, 2015, p. 512.

FIG. 1. Magnifications of moored high-resolution temperature observations under internal waves near the buoyancy frequency following a strong northerly wind event in Lake Garda (I) during early winter. Note the different greyscale-value ranges between the two panels. (a) Time-depth plot of Conservative Temperature for 3.5 h, 65 m above the lake floor. The rectangle indicates the magnification of the lower panel. The horizontal axis is at the lake floor. (b) 0.4 h, 52 m high detail of a. The horizontal scale dX is calculated using the mean mid-depth (z = -187 m) flow speed for this time-window.

FIG. 2. One inertial period (16.7 h) of high-resolution temperature observations with predominantly shear-driven overturning in the weakly stratified layer near the lake floor. (a) Time-depth plot of logarithm of buoyancy frequency with black isotherms drawn every 0.01°C. The bars on top indicate mean buoyancy period (purple), maximum buoyancy period (light-blue; close to half inertial period) and inertial period (white). The lake floor is at the horizontal axis. (b) Time-depth plot of lower 60 m of Conservative Temperature. Isotherms as in a. (c) As b., but for a different colour range highlighting the weakly stratified layer near the lake floor. Contours as in a. (d) Temperature spectra averaged over the upper 30 sensors (unsmoothed in light-blue, smoothed in red) and over the lower 30 sensors (purple, black). Several frequencies are indicated, including the local inertial frequency f, its higher harmonic 2f, semidiurnal solar S_2, and depth-(colour-)specific large-(148.5-m)-scale mean buoyancy frequency N, small-(1.5 m-)scale N_{max}, Ozmidov frequency σ_O (calculated using mid-depth mean current amplitude). The inertial subrange scaling of $\sigma^{-5/3}$ is indicated by the horizontal solid black line. Several other scalings are indicated by dashed lines and their relative slope value (for a log-log plot). (e) Coherence spectra for 1.5 m vertical separation distances averaged over all possible independent pairs of T-sensor records in the same vertical ranges and plotted for the same horizontal axis frequency range as for d. The 95% significance level is approximately at Coh = 0.2.

FIG. 3. As Fig. 2, but almost one day earlier with predominantly convection-driven overturning in the weakly stratified layer near the lake floor.

FIG. 4. Cartoons of potential generation mechanisms of internal wave induced convection. (a) Internally forced convection via downward acceleration into a near-homogeneous layer preconditioned during the preceding 'upward' wave-phase. Reduced gravity is indicated by g'. (b) Obliquely propagating internal waves (redrawn after Thorpe, 1994).

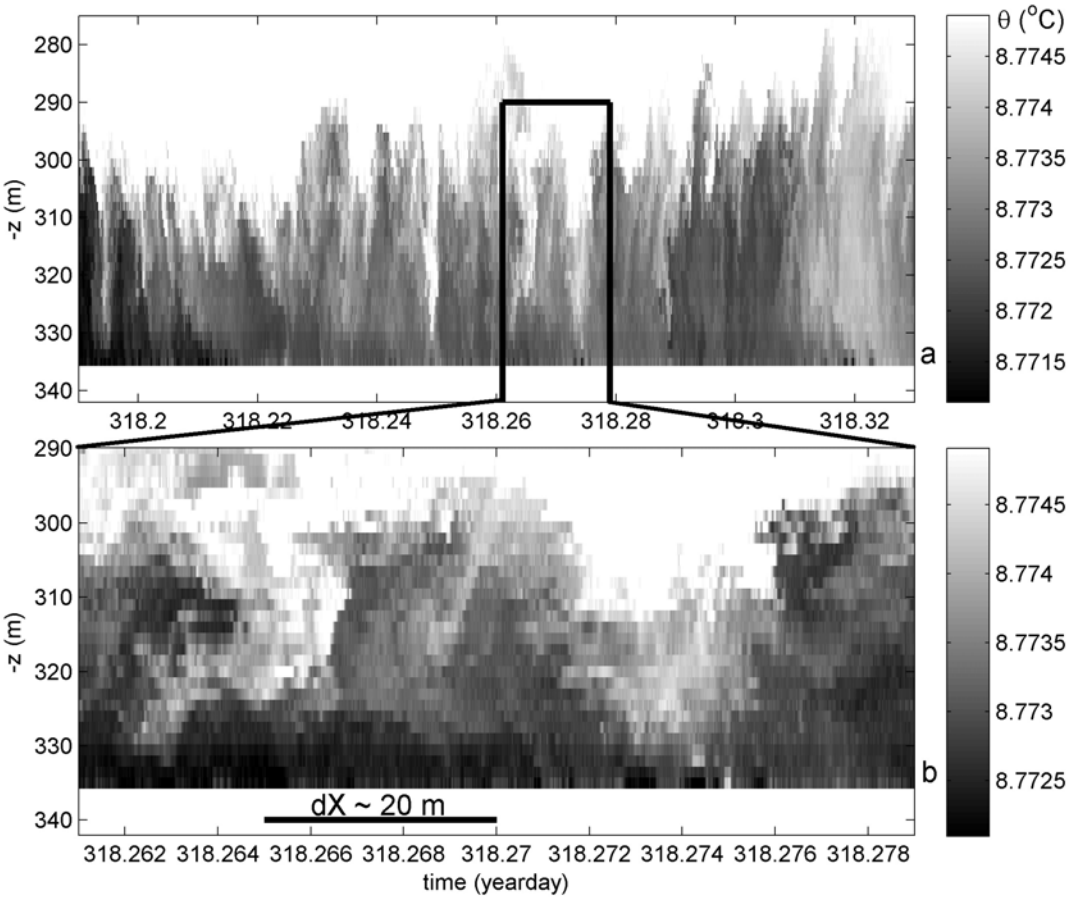

FIG. 1. Magnifications of moored high-resolution temperature observations under internal waves near the buoyancy frequency following a strong northerly wind event in Lake Garda (I) during early winter. Note the different greyscale-value ranges between the two panels. (a) Time-depth plot of Conservative Temperature for 3.5 h, 65 m above the lake floor. The rectangle indicates the magnification of the lower panel. The horizontal axis is at the lake floor. (b) 0.4 h, 52 m high detail of a. The horizontal scale dX is calculated using the mean mid-depth (z = -187 m) flow speed for this time-window.

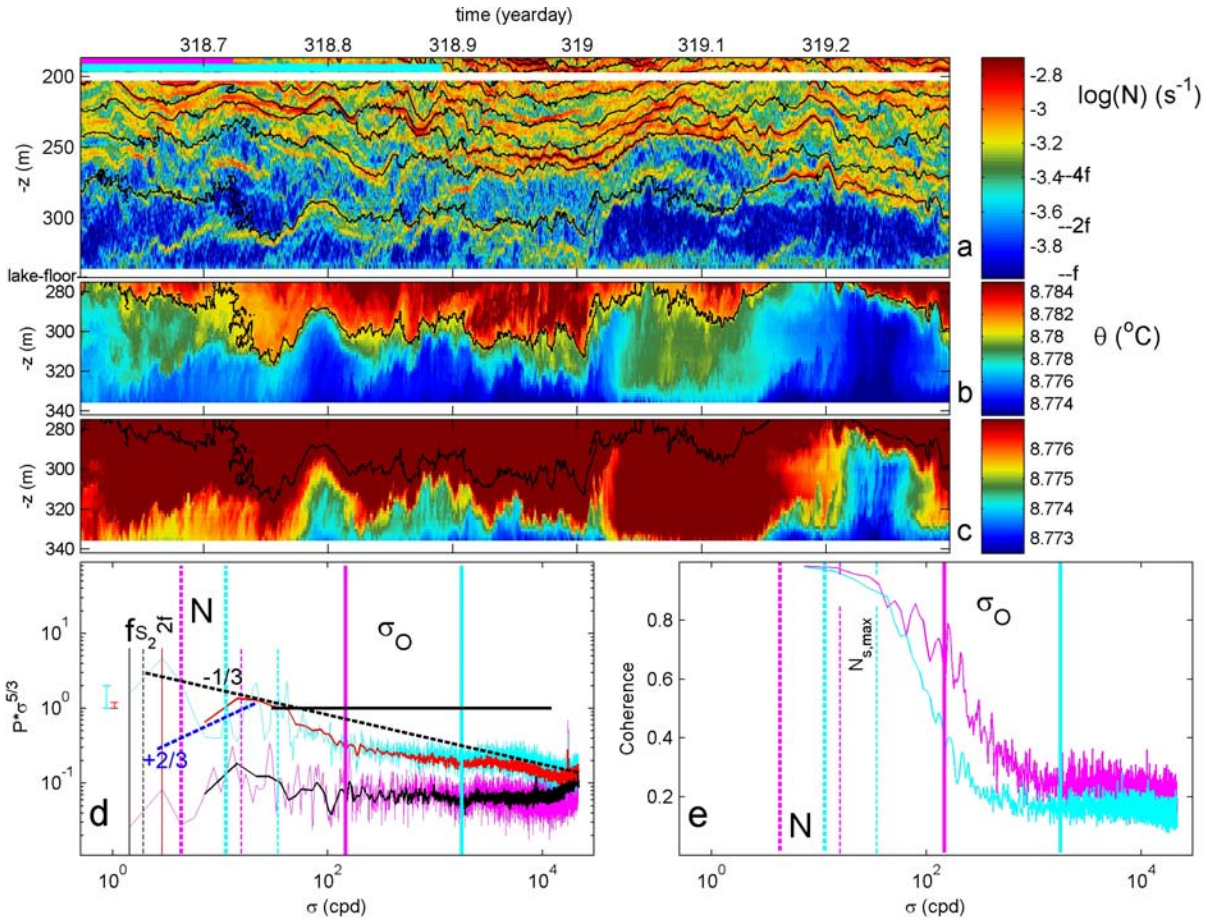

FIG. 2. One inertial period (16.7 h) of high-resolution temperature observations with predominantly shear-driven overturning in the weakly stratified layer near the lake floor. (a) Time-depth plot of logarithm of buoyancy frequency with black isotherms drawn every 0.01°C. The bars on top indicate mean buoyancy period (purple), maximum buoyancy period (light-blue; close to half inertial period) and inertial period (white). The lake floor is at the horizontal axis. (b) Time-depth plot of lower 60 m of Conservative Temperature. Isotherms as in a. (c) As b., but for a different colour range highlighting the weakly stratified layer near the lake floor. Contours as in a. (d) Temperature spectra averaged over the upper 30 sensors (unsmoothed in light-blue, smoothed in red) and over the lower 30 sensors (purple, black). Several frequencies are indicated, including the local inertial frequency f, its higher harmonic 2f, semidiurnal solar S_2, and depth-(colour-)specific large-(148.5-m)-scale mean buoyancy frequency N, small-(1.5 m-)scale N_{max}, Ozmidov frequency σ_O (calculated using mid-depth mean current amplitude). The inertial subrange scaling of $\sigma^{-5/3}$ is indicated by the horizontal solid black line. Several other scalings are indicated by dashed lines and their relative slope value (for a log-log plot). (e) Coherence spectra for 1.5 m vertical separation distances averaged over all possible independent pairs of T-sensor records in the same vertical ranges and plotted for the same horizontal axis frequency range as for d. The 95% significance level is approximately at Coh = 0.2.

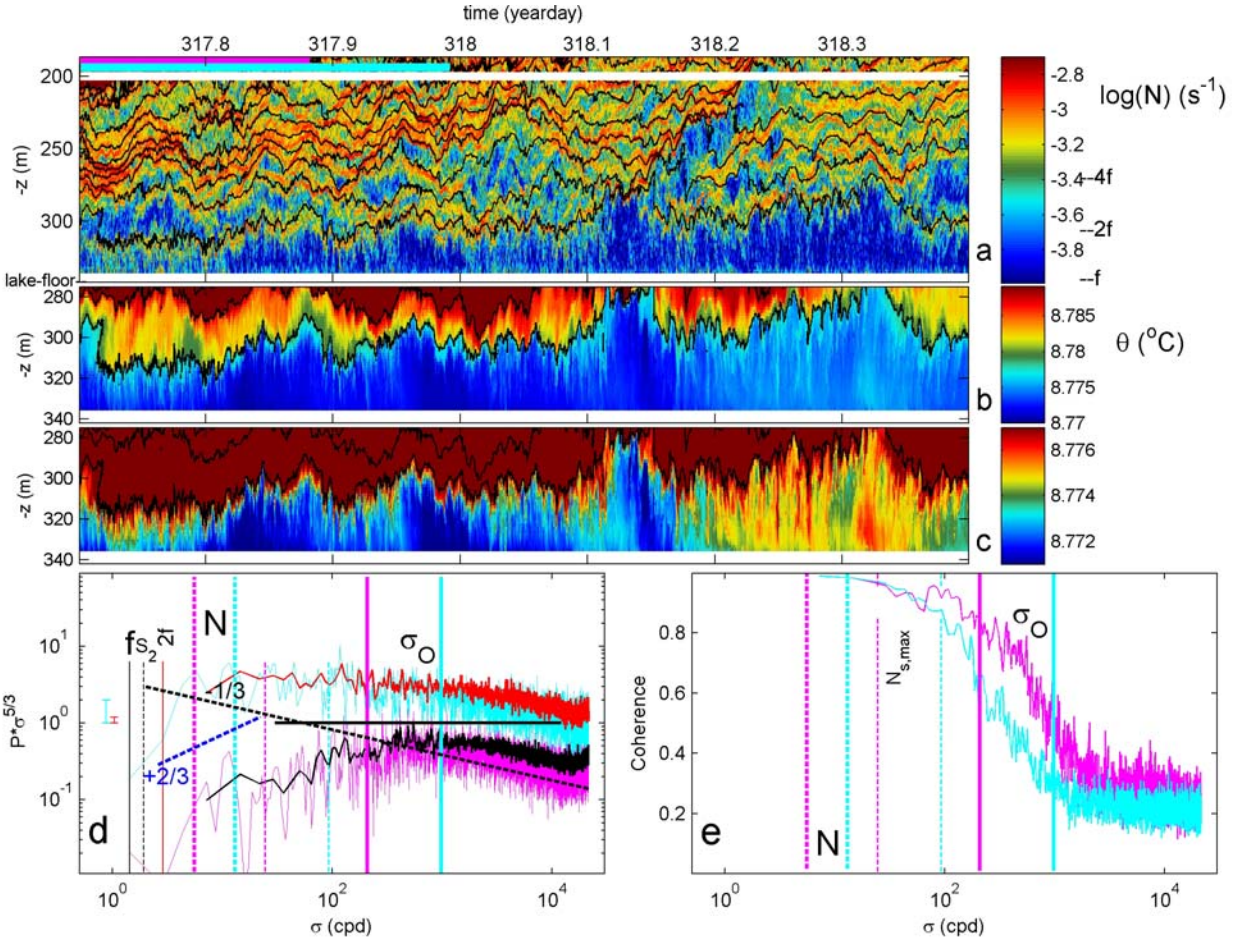

FIG. 3. As Fig. 2, but almost one day earlier with predominantly convection-driven overturning in the weakly stratified layer near the lake floor.

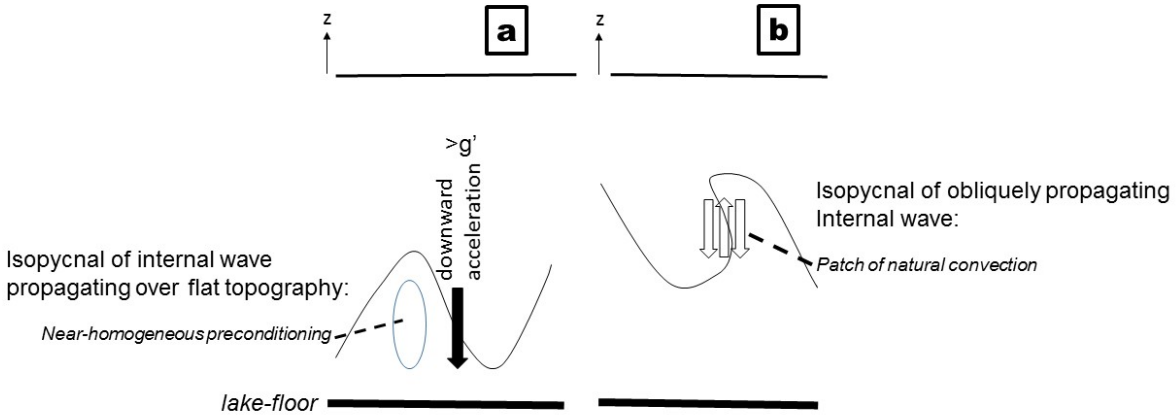

FIG. 4. Cartoons of potential generation mechanisms of internal wave induced convection. (a) Internally forced convection via downward acceleration into a near-homogeneous layer preconditioned during the preceding 'upward' wave-phase. Reduced gravity is indicated by g'. (b) Obliquely propagating internal waves (redrawn after Thorpe, 1994).